Applied Catalysis B: Environmental 224 (2018) 586–593

Contents lists available at ScienceDirect

Applied Catalysis B: Environmental

journal homepage: www.elsevier.com/locate/apcatb

Research paper

Facile synthesis of heterostructured $YVO_4/g\text{-}C_3N_4/Ag$ photocatalysts with enhanced visible-light photocatalytic performance

Yu Gao[a], Junying Lin[a], Qingzhe Zhang[b,*], He Yu[a], Fu Ding[a,*], Baotong Xu[a], Yaguang Sun[a,*], Zhenhe Xu[a,*]

[a] The Key Laboratory of Inorganic Molecule-Based Chemistry of Liaoning Province, College of Applied Chemistry, Shenyang University of Chemical Technology, Shenyang, 110142, China

[b] Institut National de la Recherche Scientifique (INRS), Centre Énergie Materiaux et Télécommunications, Université du Québec, 1650 Boulevard Lionel-Boulet, Varennes, Québec J3X1S2, Canada

ARTICLE INFO

Keywords:
YVO_4
$g\text{-}C_3N_4$
Ag
Visible light
Photocatalysis

ABSTRACT

A series of $YVO_4/g\text{-}C_3N_4/Ag$ composite photocatalysts with various concentrations of YVO_4 ($YVO_4/g\text{-}C_3N_4/Ag$) were synthesized for the first time by hydrothermal and the photodeposition method. The photocatalytic activity of the as-prepared $YVO_4/g\text{-}C_3N_4/Ag$ composites was evaluated by the degradation of methyl orange (MO) under visible light irradiation. It shows that the photocatalytic activity of $g\text{-}C_3N_4$ can be largely enhanced by loading Ag nanoparticles (NPs) and YVO_4 NPs together. The optimized loading content of YVO_4 is 35 wt%, and the highest rate constant shown in 35 *wt*% $YVO_4/g\text{-}C_3N_4/Ag$ is 0.03404 min^{-1}, about 3 times and 2.1 times higher than that in $g\text{-}C_3N_4$ (0.01131 min^{-1}) and $g\text{-}C_3N_4/Ag$ (0.01613 min^{-1}), respectively. The surface plasmon resonance (SPR) of Ag NPs and efficiently suppressed recombination of charge carriers due to the introduction of YVO_4 NPs make the $YVO_4/g\text{-}C_3N_4/Ag$ nanocomposite photocatalysts exhibit excellent visible photocatalytic performance and excellent photocatalytic stability. In addition, the trapping experiments using different scavengers showed that the reactive $O_2\cdot$ and $\cdot OH$ play the major role in the photodegradation of MO.

1. Introduction

In the modern society, energy crisis and environmental pollution have become the vital problems facing human beings [1–4]. Exploring an efficient way to solve these two problems has been one of the hottest research topics [5]. Photocatalysis is attracting more and more attention in photodegradation of organic pollutants for environmental remediation due to the redox capacity of photocatalysts driven by solar energy [1,6–9]. Up to date, considerable efforts have been made to develop green, renewable, efficient and broadband photocatalysts.

As two-dimensional (2D) nanosheets of tri-s-triazine, polymeric graphitic carbon nitride ($g\text{-}C_3N_4$) has been considered as one "sustainable" material for photocatalysis, because of its facile preparation process and the abundant and low-cost raw material [10,11]. Furthermore, being different from other polymer materials, the $g\text{-}C_3N_4$ possesses thermal stability, as well as acidic and alkaline resistance. But above all, the $g\text{-}C_3N_4$ can absorb visible light up to 450 nm due to its relatively narrow band gap (2.7 eV) [12], and has been recognized as one of the potential candidates of visible-light photocatalysts. However, there are still some shortcomings that restrict the practical applications of $g\text{-}C_3N_4$, such as the small surface area, high recombination rate of photogenerated electron-hole pairs, and the poor absorption of the visible light with the wavelength longer than 450 nm [13–16]. To address these issues, numerous strategies have been proposed to facilitate the charge carriers separation and transportation and extend the absorption range towards longer wavelengths, for example, the coupling with narrower-band gap semiconductors, doping with metallic and nonmetallic elements, and introducing carbonaceous material [17–22], *etc*.

Recently, the orthovanadates, such as $BiVO_4$, $InVO_4$ and YVO_4, *etc.*, have been studied as photocatalysts with good performance in the water splitting and/or photodegradation [23–25]. It is known that YVO_4 has a wide band gap (3.38 eV), which can only be excited by UV light, but the excited charge carriers exhibit stronger redox capability [25,26]. Therefore, the coupling of $g\text{-}C_3N_4$ with YVO_4 is a possible approach to make the composite possess improved visible-light photocatalytic activity, which has been seldom been reported yet. However, the limited range in the utilization of visible light and the fast recombination of charge carriers remain unsolved through the combination of $g\text{-}C_3N_4$ and YVO_4.

* Corresponding authors.
E-mail addresses: zhangqingzhe17@163.com (Q. Zhang), xuzh@syuct.edu.cn (Z. Xu).

http://dx.doi.org/10.1016/j.apcatb.2017.11.003
Received 28 August 2017; Received in revised form 1 November 2017; Accepted 2 November 2017
Available online 03 November 2017
0926-3373/

The noble metallic nanoparticles (NPs), such as Au and Ag, have attracted considerable attention to enhancing the visible light activity of photocatalysts due to their surface plasmon resonance (SPR) effect [27–32]. In the case of Ag/g-C_3N_4, Ag NP can broaden the light absorption of g-C_3N_4 over a wide range via the SPR effect; furthermore, Ag NP can act as the electron reservoir, promoting the transfer of charge carriers and suppress their recombination [33,34]. For example, Chen et al. reported that the photocatalytic performance of g-C_3N_4 could be enhanced by introducing the Ag NPs in the degradation of Rhodamine B [35]. Zhu et al. prepared Ag@C_3N_4 core-shell plasmonic composite and obtained enhanced photocatalytic activity originated from a combined result of the SPR effect of Ag and hybrid effect from C_3N_4 [33].

In this paper, the ternary composite of heterostructured YVO_4/g-C_3N_4/Ag photocatalyst was designed and synthesized for the first time. A series of composite photocatalysts with 2 wt% Ag and various amount of YVO_4 were prepared by the hydrothermal and photodeposition method. The composite photocatalysts exhibited enhanced photocatalytic performance in the degradation of methyl orange (MO) under visible-light irradiation (> 420 nm), remarkably suggesting that the combined effects of the SPR of Ag NPs and the coupling with YVO_4 NPs which efficiently suppress the charge carriers recombination. Moreover, the possible mechanism involved in the photocatalytic reaction was proposed in detail.

2. Experimental details

2.1. Materials

The initial chemicals, including Y_2O_3 (≥99.99%) which was purchased from GZSUNKO new material company, and other chemicals were purchased from Beijing Chemical Company, China. All chemicals were reagent grade and were used directly without further purification. Rare earth chloride stock solutions (0.2 M) were prepared by dissolving the corresponding metal oxide in HCl acid under stirring.

2.2. Preparation of YVO_4/g-C_3N_4/Ag nanocomposites

The synthesis procedures of YVO_4/g-C_3N_4/Ag nanocomposites are shown in Fig. 1. The g-C_3N_4 was obtained by calcining a certain amount of urea. Typically, 5 g of urea was placed in a covered alumina crucible and thermally treated at 550 °C for 4 h with a heating rate of 1 °C min^{-1} under air atmosphere. The yellow-colored product was collected and ground into powder for further use.

The YVO_4/g-C_3N_4 nanocomposites were prepared by a hydrothermal method. Typically, 0.25 g of g-C_3N_4 was dispersed into 20 mL of deionized water under ultrasonication for 0.5 h, and then YCl_3 solution and NH_4VO_3 were added slowly to the dispersion with the same molar of Y^{3+} and V^{5+}. After ultrasonication for another 0.5 h, the mixture was transferred into a 100 mL a Teflon bottle held in a stainless steel autoclave, sealed, and maintained at 180 °C for 6 h. After naturally cooling down to room temperature, the solid product was collected and washed thoroughly by centrifugation with deionized water, and then dried at 80 °C for 12 h. For comparison, pure YVO_4 was prepared using the same method, except for not adding g-C_3N_4 sheets to the YVO_4 solution.

The YVO_4/g-C_3N_4/Ag photocatalysts were prepared by a simple photodeposition method. As photodeposition is an appropriate approach to prevent NPs from aggregation, it can be used to prepare supported Ag NPs with highly dispersed active sites [36]. Specifically, the as-prepared YVO_4/g-C_3N_4 powder (0.10 g) was dispersed into the $AgNO_3$ aqueous solution. The resulting suspension was irradiated under a 300W Xe lamp for 2 h. Then the powder separated by centrifugation was washed with deionized water. Finally, the product was dried at 80 °C for 12 h.

2.3. Characterization

The X-ray diffraction (XRD) patterns of the samples were recorded on a D8 Focus diffractometer (Bruker) with use of Cu Kα radiation (λ = 0.154 nm). Fourier transform infrared (FT-IR) spectra were measured with a Nicolet Magna 560 infrared spectrophotometer with the KBr pellet technique. ESCALAB 250 spectrometer (Thermo Electron Corporation, UK) equipped with an Al K_α source and a charge neutralizer was used to measure X-ray photoelectron spectroscopy (XPS) and ultraviolet photoelectron spectroscopy (UPS). All the spectra were calibrated to the C1s peak at 284.6 eV of the adventitious carbon. Transmission electron microscopy (TEM) was performed by using an FEI Tecnai G^2 S–Twin instrument with a field emission gun operating at 200 kV. Images were acquired digitally on a Gatan multipole CCD camera. The UV–vis diffuse reflectance spectra (DRS) of catalysts were recorded on a UV–vis spectrometer (U-4100; HITACHI, Tokyo, Japan) equipped with an integrating sphere. The photoluminescence (PL) spectra were measured by using a fluorescence spectrophotometer (F4600, Hitachi, Japan) with the excitation wavelength of 300 nm.

2.4. Photocatalytic experiment and the detection of active species

The photocatalytic performances of the as-prepared YVO_4/g-C_3N_4/Ag photocatalysts were investigated by photodegrading MO dye in aqueous solution. 20 mg of the as-prepared photocatalysts were added to 20 mL of the MO aqueous solution (20 mg L^{-1}) in a quartz flask (50 mL in capability), and was magnetically stirred for 30 min in the dark to reach the desorption − absorption equilibrium. A 300 W xenon lamp filtered by a UV cut-off filter (λ > 420 nm) was used as the visible light source. At certain time intervals, 0.6 mL of the reaction solution was taken out and centrifuged to remove the catalyst, then analyzed on UV–vis spectrometer to detect the residual concentration of MO in the solution. In addition, in order to detect the generated active species in the photocatalysis, 1,4-benzoquinone (BQ) (1 mM), disodium ethylenediaminetetraacetate (Na_2EDTA) (1 mM), and tert-butyl alcohol (t-BuOH) (1 mM) were used as superoxide radical (·O_2^-), hole, and hydroxyl radical (·OH) scavengers, respectively, with all other conditions being the same.

3. Results and discussion

3.1. Characterization of prepared samples

The crystallinity and phase purity of the as-prepared samples were characterized by XRD (Fig. 2). For the pure YVO_4 (Fig. 2A), it can be

Fig. 1. Schematic illustration for the synthesis of the YVO_4/g-C_3N_4/Ag nanocomposite.

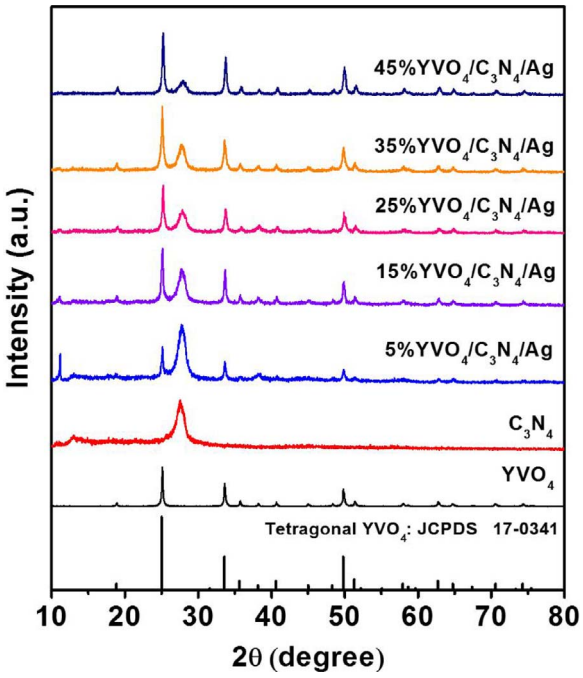

Fig. 2. XRD patterns of YVO_4, g-C_3N_4, and YVO_4/g-C_3N_4/Ag samples with different contents of YVO_4 from 15 *wt*% to 45 *wt*%.

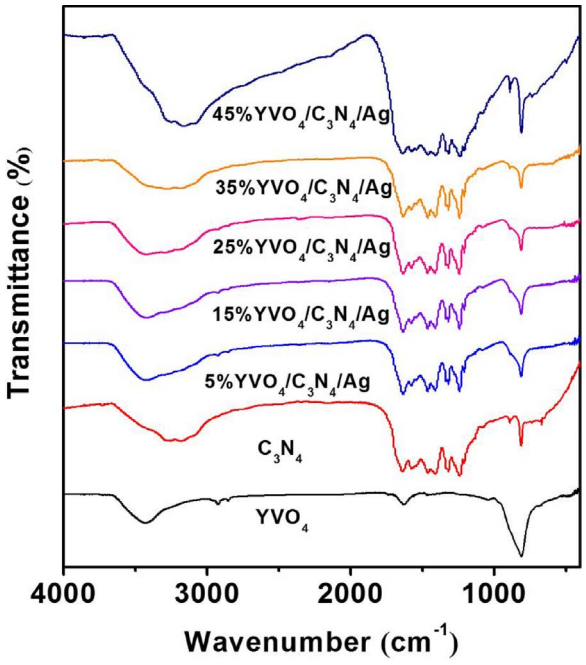

Fig. 3. FT-IR spectra of YVO_4, g-C_3N_4, and YVO_4/g-C_3N_4/Ag samples with different contents of YVO_4 from 15 *wt*% to 45 *wt*%.

seen that all the diffraction peaks of the sample can be readily indexed to a pure tetragonal phase of YVO_4 (space group: $I4_1/amd$) according to the JCPDS file No. 17-0341 (a = b = 7.1192 Å and c = 6.2898 Å). The well-resolved diffraction peaks, no peaks shifts, and other impurity phases appearance indicates the high crystallinity and purity of the as-prepared sample [37]. As for the pure g-C_3N_4 sample (Fig. 2B), it shows diffraction peaks at 13.1° and 27.4°, which can be indexed as the (100) crystal plane of tri-s-triazine units and the (002) diffraction for inter-layer stacking of aromatic systems of graphitic materials, respectively [38,39]. For the YVO_4/g-C_3N_4/Ag composites (Fig. 2C-G), the XRD patterns show YVO_4 and g-C_3N_4 phases. With an increasing amount of YVO_4 from 5.0% to 45.0%, the diffraction peaks of YVO_4 are intensified gradually, whereas the peaks of g-C_3N_4 are weakened. However, due to the quiet low loading amount and the overlapping of diffraction peaks in all these samples, the diffractions of Ag NPs could not be observed. The peaks at 27.4° in YVO_4/g-C_3N_4/Ag samples suggest that the structure of g-C_3N_4 is not changed by the hydrothermal treatment.

For further confirming the formation of the YVO_4/g-C_3N_4/Ag composites, the FT-IR spectra of the as-prepared products were also measured (Fig. 3). As shown in Fig. 3A, the YVO_4 sample has a strong characteristic peak at 820 cm^{-1}, which can be attributed to the V–O stretching vibration mode (from the VO_4^{3-} group) [40]. For the bare g-C_3N_4 sample (Fig. 3B), the peak at 812 cm^{-1} is attributed to the characteristic breathing modes of triazine units [41]. The peaks at 1641, 1580, 1465, 1404, 1323, and 1242 cm^{-1} are associated with the stretching vibrations of CN heterocycles [42]. The broad peak at 3000–3650 cm^{-1} was assigned to the stretching vibration modes of terminal N—H and O—H [43]. All the YVO_4/g-C_3N_4/Ag composites exhibit similar peaks as the g-C_3N_4 sample. With the increase of YVO_4 amount, this band was affected and shifted towards the higher wavenumber due to the presence of the absorption band of YVO_4 at 820 cm^{-1}. This is another evidence for the introduction of YVO_4 into g-C_3N_4.

The surface chemical composition and status of elements in the YVO_4/g-C_3N_4/Ag sample were further analyzed by XPS (Fig. 4). Fig. 4a shows the XPS survey spectrum of the YVO_4/g-C_3N_4/Ag composite, which suggests that sample primarily consists of Y, V, O, C, N and Ag elements without other impurities. As displayed in Fig. 4B, the V2p states split into two lines $V2p_{1/2}$ (524.6 eV) and $V2p_{3/2}$ (517.1 eV) with an energy splitting of 7.5 eV because of the spin-orbit interactions [44,45]. In addition, the difference of binding energy between the $V2p_{3/2}$ and the O 1 s (530.0 eV) is about 12.9 eV, confirming the presence of V^{5+} oxidation state [44]. Fig. 4C shows that the Y3d state was fitted into two peaks, $Y3d_{3/2}$ (159.3 eV), and $Y3d_{5/2}$ (157.2 eV). Meanwhile, the ultraviolet photoelectron spectroscopy (UPS) was carried out to determine the VB position of YVO_4 (Fig. 4D). The VB maximum potential was calculated to be 2.61 eV, which is consistent with the previously reported work [44].

The morphology and microstructure of the as-prepared samples were further observed by TEM technique (Fig. 5). For YVO_4 sample (Fig. 5A), irregularly shaped nanoparticles can be observed. Fig. 5B shows the typical TEM image of g-C_3N_4, which exhibited 2D sheet-like nanostructures with transparent thin layers resembling the graphene nanosheets. Upon incorporating Ag NPs, the TEM image (Fig. 5C) shows that the Ag NPs are uniformly dispersed on the surface of g-C_3N_4 nanosheets. The YVO_4/g-C_3N_4/Ag composite with the YVO_4 NPs and Ag NPs supported on the g-C_3N_4 nanosheets is displayed in Fig. 5D. It can be seen that the YVO_4 NPs and Ag NPs were randomly distributed on the surface of g-C_3N_4 sheets. The TEM characterization also confirms the successful synthesis of YVO_4/g-C_3N_4/Ag composites, which are consistent with the XRD and FT-IR analysis. The high-resolution TEM (HRTEM) image of YVO_4/g-C_3N_4/Ag displays the interface and spatial arrangement of these three components (Fig. 5E). The lattice fringes with inter-plane distances of 0.32 nm and 0.24 nm correspond to the (200) planes in the tetragonal YVO_4 structure [46], and the (111) plane of the face-centered cubic Ag NPs [47], respectively. Furthermore, the YVO_4/g-C_3N_4/Ag composite was ultra-sonicated for 1 h for TEM analysis, indicating that the interaction among these three components is very strong, which is particularly favorable for the photocatalysis.

The optical absorption properties of all the samples were measured by the UV–vis spectrometer (Fig. 6). Fig. 6A shows the UV–vis absorption spectra of pure g-C_3N_4, g-C_3N_4/Ag and the YVO_4/g-C_3N_4/Ag with different YVO_4 contents. A shown in the absorption spectra, pure g-C_3N_4 and all the samples contain g-C_3N_4 show visible light absorption with absorption edge around 465 nm. For the samples with Ag, the extra broad absorption band centers at ~500 nm was also observed,

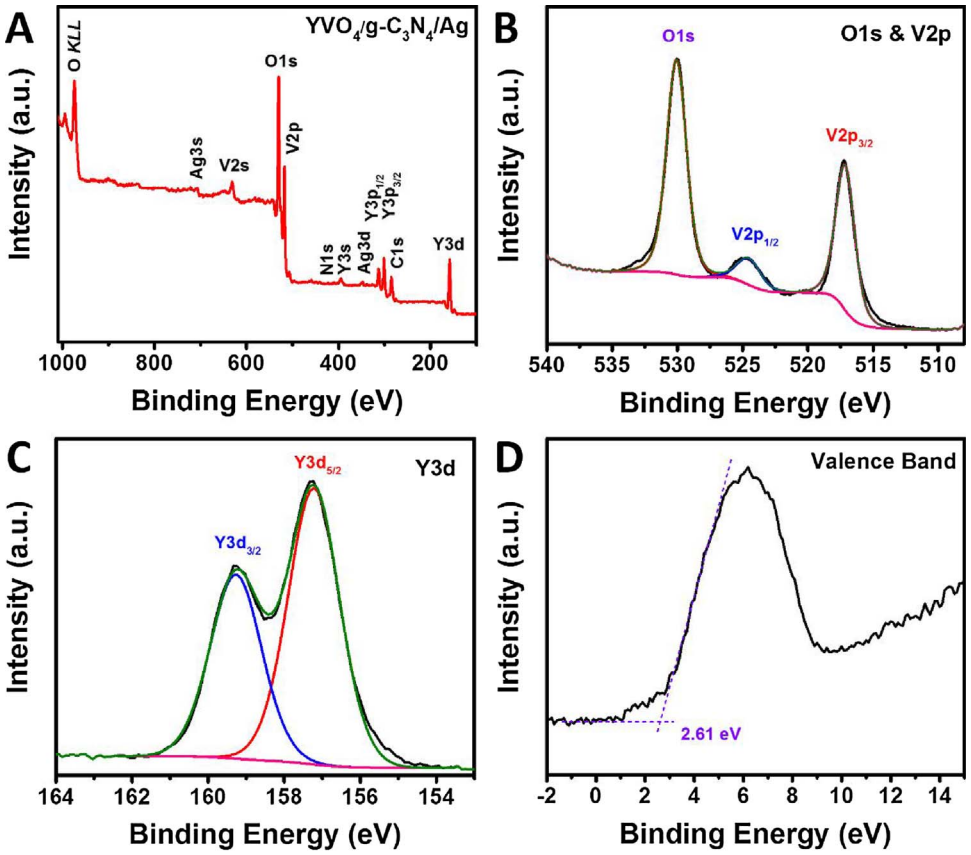

Fig. 4. (A) XPS survey spectra, (B) high-resolution O1 s and V2p, (C) high-resolution Y3d of YVO_4/g-C_3N_4/Ag, and (D) UPS spectrum of YVO_4 to determine its VB position.

which is attributed to the SPR of Ag NPs [48–50]. As shown in Fig. 6B, the YVO_4 can only absorb the UV light with the absorption edge around 363 nm. According to the Kubelka-Munk function [39], the band gap energy of YVO_4 can be estimated to be 3.42 eV. Considering that the VB maximum of YVO_4 is 2.61 eV and its band gap energy is 3.42 eV, the CB minimum is calculated to be −0.81 eV.

3.2. Photocatalytic performance

The photocatalytic activity of YVO_4/g-C_3N_4/Ag composite was assessed by the photodegradation of MO at room temperature under visible light ($\lambda > 420$ nm) irradiation. Meanwhile, we also tested the blank experiment under the same condition to investigate the photostability and chemical stability of MO. After 120 min, no MO was degraded without the help of the photocatalyst, indicating that MO is a suitable model dye with high stability under visible light irradiation. Fig. 6A shows the decrease of MO concentration as a function of time over different photocatalysts. The concentration of MO is unchanged after 2 h in the presence of YVO_4 under visible light irradiation. As expected, the g-C_3N_4 and g-C_3N_4/Ag show visible light activity in the

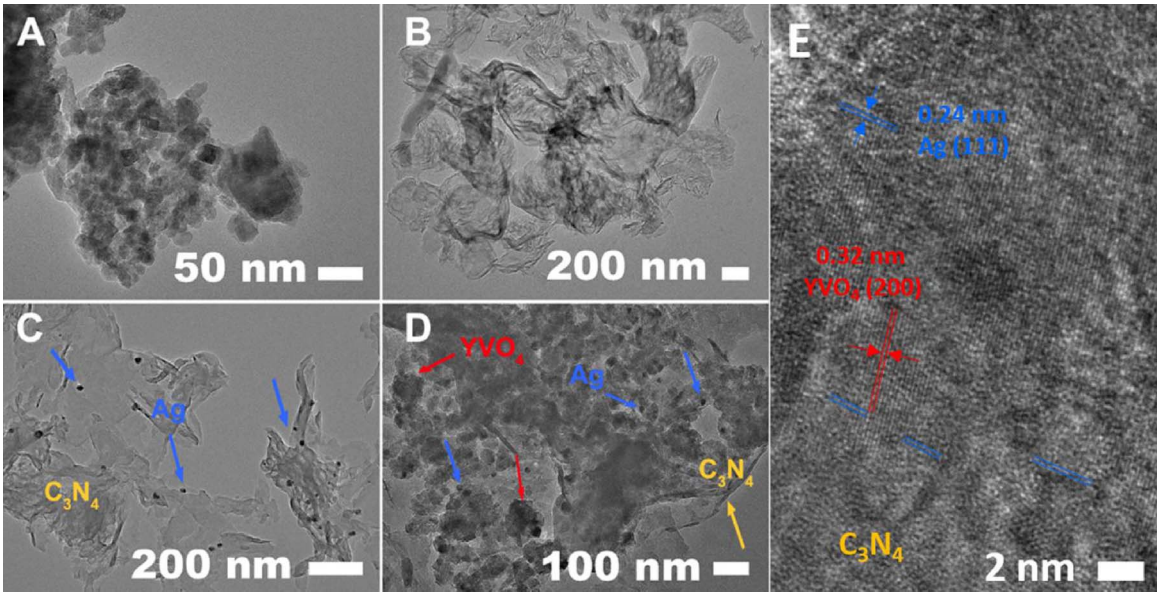

Fig. 5. TEM images of (A) YVO_4, (B) g-C_3N_4, (C) g-C_3N_4/Ag, (D) YVO_4/g-C_3N_4/Ag, and (E) HRTEM image of YVO_4/g-C_3N_4/Ag sample.

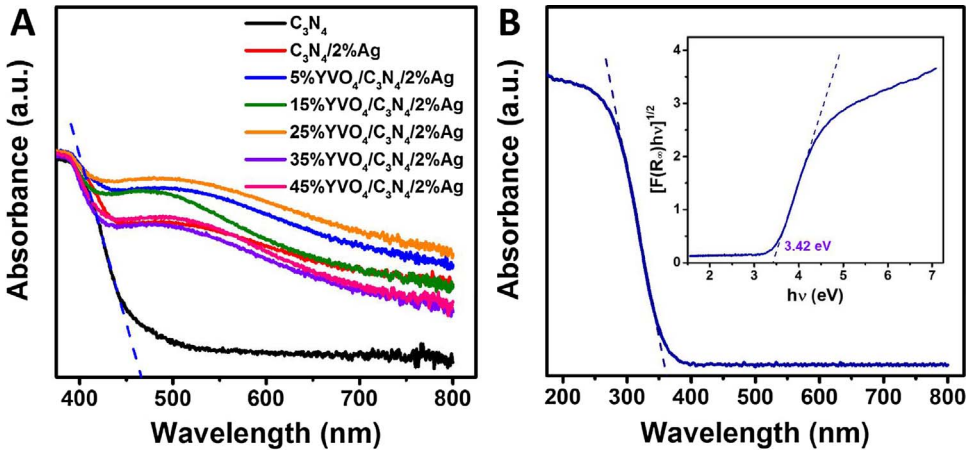

Fig. 6. Absorption spectra of (A) g-C_3N_4 and YVO_4/g-C_3N_4/Ag samples with different contents of YVO_4 from 15 *wt*% to 45 *wt*%, and (B) YVO_4 sample. The inset in (B) is the $(\alpha h\nu)^2$ *vs* $h\nu$ curve to calculate the band gap of YVO_4.

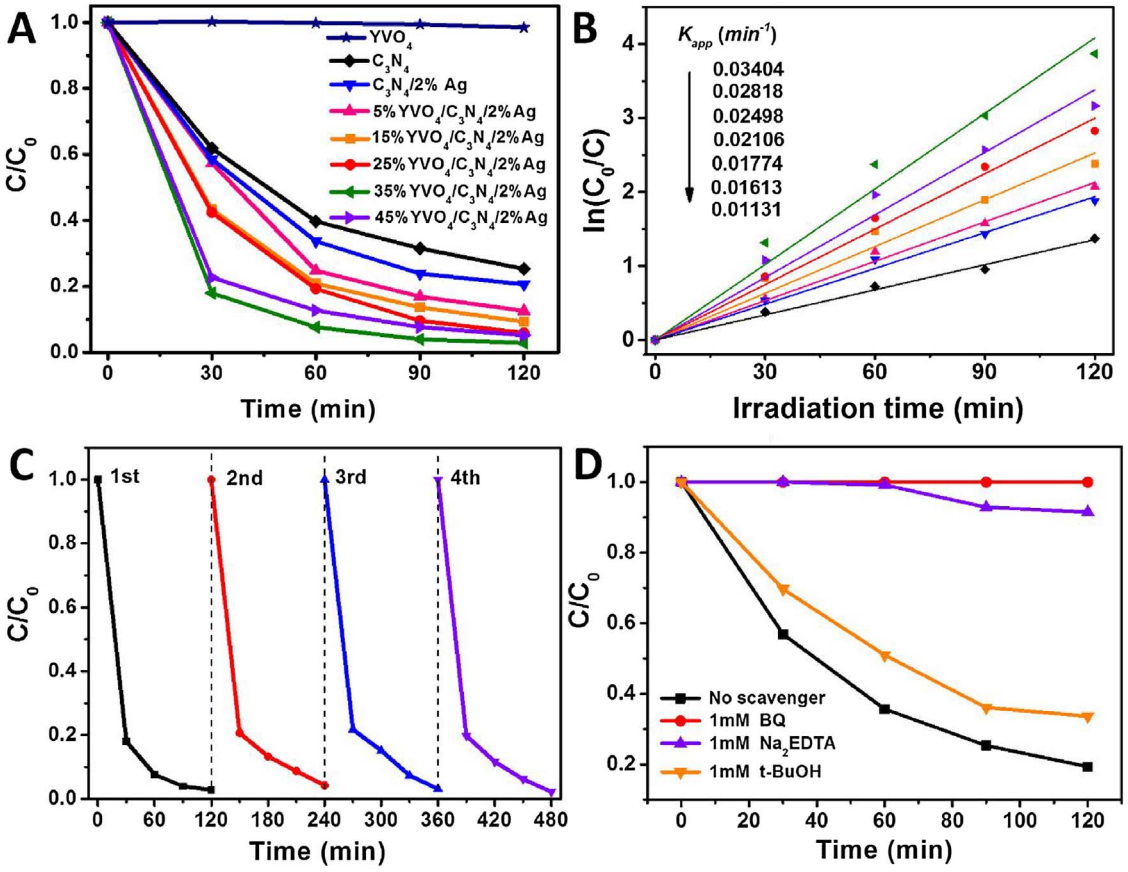

Fig. 7. (A) The photodegradation activities of MO as a function of time over different photocatalysts under visible light irradiation, (B) plot of $\ln(c_0/c)$ *vs* time and the apparent reaction rate constant, (C) cycling runs of 35 *wt*%YVO_4/g-C_3N_4/Ag photocatalyst in the photodegradation of MO, and (D) photodegradation of MO in the presence of three types of scavengers and 35 *wt*%YVO_4/g-C_3N_4/Ag photocatalyst under visible light irradiation.

photocatalytic degradation of MO. After the introduction of YVO_4, the photocatalytic degradation rate was increased compared with the g-C_3N_4 and g-C_3N_4/Ag samples, because of the restrained recombination of charge carriers. The optimal content of YVO_4 in YVO_4/g-C_3N_4/Ag was found to be 35 *wt*% by comparing their photocatalytic efficiency in the degradation of MO solution.

With increasing the concentration of YVO_4 over 35%, the photocatalytic degradation rate starts to decrease, which is because that the covering of excessive YVO_4 on the surface of g-C_3N_4 leads to the poor optical penetration.

For the kinetic study of different photocatalysts, the photocatalysis data were fitted with the pseudo-first-order model (Fig. 5B). The equation is $\ln(C_0/C) = kt$, where C_0 and C are the concentrations of MO at irradiation time of 0 and t, respectively, and k is the apparent reaction rate constant. Fig. 5B shows that the photocatalytic degradation of MO, in the presence of as-prepared photocatalysts under visible light irradiation, which matches well with the pseudo-first-order model. As displayed in Fig. 5C, the highest rate constant (0.03404 min^{-1}) is achieved by the 35% YVO_4/g-C_3N_4/Ag sample, which is about 3 times higher than the pure g-C_3N_4 sample (0.01131 min^{-1}), and about 2.1 times higher than the g-C_3N_4/Ag sample (0.01613 min^{-1}). To be served as a good photocatalyst, except for the enhanced visible light activity, the reusability and stability are also extremely important. The photocatalytic degradation of MO under visible light was carried out for 4

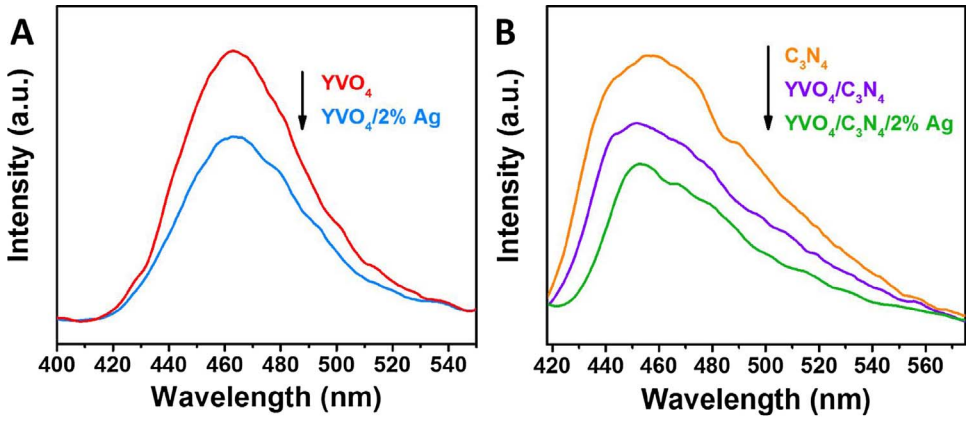

Fig. 8. PL spectra of the (A) YVO_4 and YVO_4/Ag samples, and (B) g-C_3N_4, YVO_4/g-C_3N_4 and 35 *wt*% YVO_4/g-C_3N_4/Ag samples.

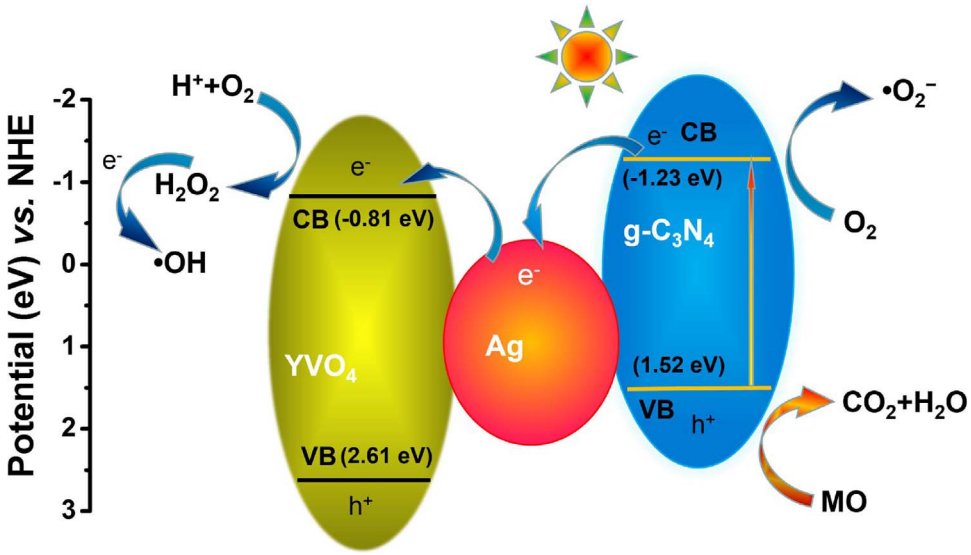

Fig. 9. Photocatalytic mechanism scheme over YVO_4/g-C_3N_4/Ag photocatalyst under visible-light irradiation.

cycles in the presence of 35% YVO_4/g-C_3N_4/Ag photocatalyst (Fig. 5C). After 4 consecutive cycles, the 35% YVO_4/g-C_3N_4/Ag still shows very high photocatalytic degradation rate of MO. This result indicates that the as-prepared YVO_4/g-C_3N_4/Ag photocatalyst possesses excellent reusability and photostability.

In order to detect the main active species in the photocatalytic process, such as photogenerated holes, superoxide radicals ($\cdot O_2^-$) and hydroxyl radicals (·OH), the trapping experiments in the presence of various scavengers were operated. As shown in Fig. 7, under the visible light irradiation of the as-prepared YVO_4/g-C_3N_4/Ag photocatalyst, the photodegradation rate of MO was slightly suppressed by the addition of ·OH radical scavenger (t-BuOH, 1 mM), which reveals that ·OH radicals are not the main active species for the photodegradation of MO in current photocatalytic systems. However, in the presence of the $\cdot O_2^-$ radical scavenger (BQ, 1 mM) and the hole scavenger (Na_2EDTA, 1 mM), the photodegradation rate of MO was decelerated significantly, with the photocatalytic degradation rate being reduced by 67.2% and 37.1%, respectively. It means that the $\cdot O_2^-$ and ·OH radicals play the major roles in the photodegradation of MO over the as-prepared YVO_4/g-C_3N_4/Ag photocatalyst under visible light irradiation.

The PL spectra are widely employed to evaluate the separation efficiency of charge carriers in photocatalysts [51–53]. The PL spectra of YVO_4, YVO_4/Ag, g-C_3N_4, YVO_4/g-C_3N_4 and 35 *wt*%YVO_4/g-C_3N_4/Ag samples are shown in Fig. 8. After 300 nm excitation, all samples exhibit broad emission peaks in the range of 400–550 nm, representing that the photo-excited electrons recombine with holes. As shown in Fig. 8A, the PL intensity decreases after the introduction of Ag NPs. As for the g-C_3N_4 sample, the loading of YVO_4 and Ag NPs both make the PL emissions quench (Fig. 8B), which indicates that the charge carries recombination in 35 *wt*%YVO_4/g-C_3N_4/Ag was largely suppressed compared with g-C_3N_4 or YVO_4.

3.3. Possible photocatalytic mechanism

On the basis of the above experimental results, the possible mechanism of photocatalytic degradation of MO under visible light irradiation is proposed (Fig. 9). According to the published work, the VB maximum and CB minimum potentials of g-C_3N_4 were at +1.52 eV and −1.23 eV [25,39], whereas the VB and CB edge potentials of YVO_4 were calculated by the combination of the band gap and UPS measurement to be at −0.81 and +2.61 eV, respectively. For the YVO_4/g-C_3N_4 sample, under visible light irradiation, only the electrons in the VB of g-C_3N_4 can be excited to the CB of g-C_3N_4 and partially react with O_2 directly to produce $\cdot O_2^-$ radicals [51–53]. Due to the difference between the CB edge potentials of g-C_3N_4 and YVO_4, the excited electrons can be easily transferred from the CB of g-C_3N_4 to the CB of YVO_4, greatly suppressing the recombination of photoinduced electrons and holes. For the YVO_4/g-C_3N_4/Ag composites, Ag NPs are deposited on the surface of YVO_4 and can act as an electron transportation bridge to facilitate the efficient separation of charge carriers in g-C_3N_4 [39]. Moreover, the deposition of Ag NPs can significantly enhance the visible-light absorption due to the SPR effect [31,39,54]. As the electrons in the CB of YVO_4 has more negative potential (-0.81 eV) than O_2/$\cdot O_2^-$ (−0.33 eV), the electrons were used for the production of $\cdot O_2^-$

radicals by reacting with O_2. The produced $\cdot O_2^-$ can accept another electron from H^+ to form H_2O_2, which can be further activated to ·OH radicals [55,56]. The electrons in the CB of YVO_4 can also directly react with adsorbed O_2 in the presence of H^+ to generate H_2O_2 and then produce ·OH radicals [51–53]. The holes left in the VB of g-C_3N_4 can directly attack the MO. With increasing the loading amount of YVO_4 over 35 wt%, the excessive YVO_4 could cover the surface of g-C_3N_4 and limited the light hitting the surface of g-C_3N_4. Hence, the optimal loading amount of YVO_4 in the YVO_4/g-C_3N_4/Ag sample is 35 wt%.

4. Conclusions

In summary, a series of novel YVO_4/g-C_3N_4/Ag composite photocatalyst with different contents of YVO_4 were successfully synthesized by a simple hydrothermal and photodeposition approach. The as-prepared composite shows excellent visible light photocatalytic performance and reusability in the degradation of MO due to the SPR effect of Ag NP as well as the charge transfer between the three components. The loading amount of YVO_4 was optimized and 35% YVO_4/g-C_3N_4/Ag sample exhibited the highest degradation rate of MO. The possible mechanism of the photocatalytic reaction was also proposed. Based on the results, the YVO_4/g-C_3N_4/Ag composite is expected to be an effective visible-light photocatalyst for environmental remediation.

Acknowledgments

This work was supported by the National Natural Science Foundation of China (NSFC 51402198, 21671139), the Natural Science Foundation of Liaoning Province (201602592, 20170540715), Educational Bureau of Liaoning Province for the Fundamental Research of Key Lab (Grand NO. LZ2014028, LZ2016003).

References

[1] H.L. Wang, L.S. Zhang, Z.G. Chen, J.Q. Hu, S.J. Li, Z.H. Wang, J.S. Liu, X.C. Wang, Semiconductor heterojunction photocatalysts: design, construction, and photocatalytic performances, Chem. Soc. Rev. 43 (2014) 5234–5244.
[2] Q. Li, B.D. Guo, J.G. Yu, J.R. Ran, B.H. Zhang, H.J. Yan, J.R. Gong, Highly efficient visible-light-driven photocatalytic hydrogen production of CdS-cluster-decorated graphene Nanosheets, J. Am. Chem. Soc. 133 (2011) 10878–10884.
[3] S.W. Cao, J.X. Low, J.G. Yu, M. Jaroniec, Polymeric photocatalysts based on graphitic carbon nitride, Adv. Mater. 27 (2015) 2150–2176.
[4] Y.X. Yang, Y.N. Guo, F.Y. Liu, X. Yuan, Y.H. Guo, S.Q. Zhang, W. Guo, M.X. Huo, Preparation and enhanced visible-light photocatalytic activity of silver deposited graphitic carbon nitride plasmonic photocatalyst, Appl. Catal. B 142 (2013) 828–837.
[5] P. Zhang, T. Wang, X.X. Chang, J.L. Gong, Effective charge carrier utilization in photocatalytic conversions, Acc. Chem. Res. 49 (2016) 911–921.
[6] G. Zhang, G. Kim, W. Choi, Visible light driven photocatalysis mediated via ligand-to-metal charge transfer (LMCT): an alternative approach to solar activation of titania, Energy Environ. Sci. 7 (2014) 954–966.
[7] W. Liu, W. Mu, M.J. Liu, X.D. Zhang, H.L. Cai, Y.L. Deng, Solar-induced direct biomass-to-electricity hybrid fuel cell using polyoxometalates as photocatalyst and charge carrier, Nat. Commun. 5 (2014) 3208.
[8] G. Wang, Q.H. Chen, Y.J. Xin, Y.P. Liu, Z.L. Zang, C.G. Hu, B. Zhang, Construction of graphene-WO_3/TiO_2 nanotube array photoelectrodes and its enhanced performance for photocatalytic degradation of dimethyl phthalate, Electrochim. Acta 222 (2016) 1903–1913.
[9] Q.H. Chen, S.N. Wu, Y.J. Xin, Synthesis of Au-CuS-TiO_2 nanobelts photocatalyst for efficient photocatalytic degradation of antibiotic oxytetracycline, Chem. Eng. J. 302 (2016) 377–387.
[10] Y. Zheng, J. Liu, J. Liang, M. Jaroniec, S.Z. Qiao, Graphitic carbon nitride materials: controllable synthesis and applications in fuel cells and photocatalysis, Energy Environ. Sci. 5 (2012) 6717–6731.
[11] X.C. Wang, K. Maeda, A. Thomas, K. Takanabe, G. Xin, J.M. Carlsson, K. Domen, M. Antonietti, A metal-free polymeric photocatalyst for hydrogen production from water under visible light, Nat. Mater. 8 (2009) 76–80.
[12] S.A. Shevlin, Z.X. Guo, Anionic dopants for improved optical absorption and enhanced photocatalytic hydrogen production in graphitic carbon nitride, Chem. Mater. 28 (2016) 7250–7256.
[13] Y. Wang, J.S. Zhang, X.C. Wang, M. Antonietti, H.R. Li, Boron- and fluorine-containing mesoporous carbon nitride polymers: metal-free catalysts for cyclohexane oxidation, Angew. Chem. Int. Ed. 49 (2010) 3356–3359.
[14] Z.H. Xu, M. Quintanilla, F. Vetrone, A.O. Govorov, M. Chaker, D.L. Ma, Harvesting lost photons: plasmon and upconversion enhanced broadband photocatalytic activity in Core@Shell microspheres based on lanthanide-doped $NaYF_4$, TiO_2, and Au, Adv. Func. Mater. 25 (2015) 2950–2960.
[15] Q.Z. Zhang, N. Bao, X.Q. Wang, X.D. Hu, X.H. Miao, M. Chaker, D.L. Ma, Advanced fabrication of chemically bonded Graphene/TiO_2 continuous fibers with enhanced broadband photocatalytic properties and involved mechanisms exploration, Sci. Rep. 6 (2016) 38066.
[16] C.T. Dinh, H. Yen, F. Kleitz, T.O. Do, Three-Dimensional ordered assembly of thin-shell Au/TiO_2 hollow nanospheres for enhanced visible-light-driven photocatalysis, Angew. Chem. Int. Ed. 53 (2014) 6618–6623.
[17] J. Schneider, M. Matsuoka, M. Takeuchi, J.L. Zhang, Y. Horiuchi, M. Anpo, D.W. Bahnemann, Understanding TiO2 photocatalysis: mechanisms and materials, Chem. Rev. 114 (2014) 9919–9986.
[18] R. Asahi, T. Morikawa, H. Irie, T. Ohwaki, Nitrogen-doped titanium dioxide as visible-light-sensitive photocatalyst: designs, developments, and prospects, Chem. Rev. 114 (2014) 9824–9852.
[19] Q.Z. Zhang, N. Bao, X.W. Zhu, D. Ma, Y.J. Xin, Preparation and photocatalytic properties of graphene/TiO_2 nanotube arrays photoelectrodes, J. Alloys Compd. 618 (2015) 761–767.
[20] A. Akhundi, A. Habibi-Yangjeh, Novel g-C_3N_4/Ag_2SO_4 nanocomposites: fast microwave-assisted preparation and enhanced photocatalytic performance towards degradation of organic pollutants under visible light, J. Colloid Interface Sci. 482 (2016) 165–174.
[21] M. Mousavi, A. Habibi-Yangjeh, M. Abitorabi, Fabrication of novel magnetically separable nanocomposites using graphitic carbon nitride, silver phosphate and silver chloride and their applications in photocatalytic removal of different pollutants using visible-light irradiation, J. Colloid Interface Sci. 480 (2016) 218–231.
[22] A. Akhundi, A. Habibi-Yangjeh, Facile preparation of novel quaternary g-C_3N_4/Fe_3O_4/AgI/Bi_2S_3 nanocomposites: magnetically separable visible-light-driven photocatalysts with significantly enhanced activity, RSC Adv. 6 (2016) 106572–106583.
[23] R.G. Li, F.X. Zhang, D.G. Wang, J.X. Yang, M.R. Li, J. Zhu, X. Zhou, H.X. Han, C. Li, Spatial separation of photogenerated electrons and holes among {010} and {110} crystal facets of $BiVO_4$, Nat. Commun. 4 (2013).
[24] K.M. Ji, J.G. Deng, H.J. Zang, J.H. Han, H. Arandiyan, H.X. Dai, Fabrication and high photocatalytic performance of noble metal nanoparticles supported on 3DOM $InVO_4$-$BiVO_4$ for the visible-light-driven degradation of rhodamine B and methylene blue, Appl. Catal. B 165 (2015) 285–295.
[25] J. Cai, Y.M. He, X.X. Wang, L.H. Zhang, L.Z. Dong, H.J. Lin, L.H. Zhao, X.D. Yi, W.Z. Weng, H.L. Wan, Photodegradation of RhB over YVO_4/g-C_3N_4 composites under visible light irradiation, RSC Adv. 3 (2013) 20862–20868.
[26] R.M. Mohamed, E.S. Aazam, Novel Ag/YVO_4 nanoparticles prepared by a hydrothermal method for photocatalytic degradation of methylene-blue dye, J. Ind. Eng. Chem. 20 (2014) 4377–4381.
[27] Z.H. Xu, Y.L. Liu, F.Q. Ren, F. Yang, D.L. Ma, Development of functional nanostructures and their applications in catalysis and solar cells, Coord. Chem. Rev. 320 (2016) 153–180.
[28] Q. Zhang, D.T. Gangadharan, Y. Liu, Z. Xu, M. Chaker, D. Ma, Recent advancements in plasmon-enhanced visible light-driven water splitting, J. Materiomics 3 (2017) 33–50.
[29] D. Mateo, I. Esteve-Adell, J. Albero, J.F.S. Royo, A. Primo, H. Garcia, 111 oriented gold nanoplatelets on multilayer graphene as visible light photocatalyst for overall water splitting, Nat. Commun 7 (2016) 11819.
[30] Z.Z. Lou, M. Fujitsuka, T. Majima, Pt-Au triangular nanoprisms with strong dipole plasmon resonance for hydrogen generation studied by single-particle spectroscopy, ACS Nano 10 (2016) 6299–6305.
[31] S. Linic, P. Christopher, D.B. Ingram, Plasmonic-metal nanostructures for efficient conversion of solar to chemical energy, Nat. Mater. 10 (2011) 911–921.
[32] Q. Zhang, J. Deng, Z. Xu, M. Chaker, D. Ma, High-efficiency broadband C_3N_4 photocatalysts: synergistic effects from upconversion and plasmons, ACS Catal. 7 (2017) 6225–6234.
[33] X.J. Bai, R.L. Zong, C.X. Li, D. Liu, Y.F. Liu, Y.F. Zhu, Enhancement of visible photocatalytic activity via Ag@C3N4 core-shell plasmonic composite, Appl. Catal. B 147 (2014) 82–91.
[34] K. Tian, W.J. Liu, H. Jiang, Comparative investigation on photoreactivity and mechanism of biogenic and chemosythetic Ag/C_3N_4 composites under visible light irradiation, ACS Sustain. Chem. Eng. 3 (2015) 269–276.
[35] Y.Y. Bu, Z.Y. Chen, W.B. Li, Using electrochemical methods to study the promotion mechanism of the photoelectric conversion performance of Ag-modified mesoporous g-C_3N_4 heterojunction material, Appl. Catal. B 144 (2014) 622–630.
[36] W. Zhang, L. Zhou, H.P. Deng, Ag modified g-C_3N_4 composites with enhanced visible-light photocatalytic activity for diclofenac degradation, J. Mol. Catal. A: Chem. 423 (2016) 270–276.
[37] Z.H. Xu, X.J. Kang, C.X. Li, Z.Y. Hou, C.M. Zhang, D.M. Yang, G.G. Li, J. Lin, Ln^{3+} (Ln = Eu, Dy, Sm, and Er) ion-doped YVO_4 Nano/Microcrystals with multiform morphologies: hydrothermal synthesis, growing mechanism, and luminescent properties, Inorg. Chem. 49 (2010) 6706–6715.
[38] M. Groenewolt, M. Antonietti, Synthesis of g-C_3N_4 nanoparticles in mesoporous silica host matrices, Adv. Mater. 17 (2005) 1789–1792.
[39] Y.F. Chen, W.X. Huang, D.L. He, S.T. Yue, H. Huang, Construction of heterostructured g-C_3N_4/Ag/TiO_2 microspheres with enhanced photocatalysis performance under visible-light irradiation, ACS Appl. Mater. Interfaces 6 (2014) 14405–14414.
[40] Z.H. Xu, S.S. Bian, T. Liu, L.M. Wang, Y. Gao, H.Z. Lian, J. Lin, Self-assembled growth of $LuVO_4$ nanoleaves: hydrothermal synthesis, morphology evolution, and luminescence properties, RSC Adv. 2 (2012) 11067–11077.
[41] Y.J. Wang, R. Shi, J. Lin, Y.F. Zhu, Enhancement of photocurrent and photocatalytic

activity of ZnO hybridized with graphite-like C_3N_4, Energy Environ. Sci. 4 (2011) 2922–2929.
[42] S.C. Yan, S.B. Lv, Z.S. Li, Z.G. Zou, Organic-inorganic composite photocatalyst of g-C_3N_4 and TaON with improved visible light photocatalytic activities, Dalton Trans. 39 (2010) 1488–1491.
[43] Y.C. Zhao, Z. Liu, W.G. Chu, L. Song, Z.X. Zhang, D.L. Yu, Y.J. Tian, S.S. Xie, L.F. Sun, Large-scale synthesis of nitrogen-rich carbon nitride microfibers by using graphitic carbon nitride as precursor, Adv. Mater. 20 (2008) 1777–1781.
[44] M. Kruczek, E. Talik, H. Sakowska, W. Szyrski, Z. Ujma, D. Skrzypek, XPS investigations of YVO_4: Tm,Yb single crystal, J. Cryst. Growth 275 (2005) E1715–E1720.
[45] Y.C. Chen, Y.C. Wu, D.Y. Wang, T.M. Chen, Controlled synthesis and luminescent properties of monodispersed PEI-modified YVO_4:Bi^{3+},Eu^{3+} nanocrystals by a facile hydrothermal process, J. Mater. Chem. A 22 (2012) 7961–7969.
[46] J.F. Liu, Y.D. Li, General synthesis of colloidal rare earth orthovanadate nanocrystals, J. Mater. Chem. 17 (2007) 1797–1803.
[47] V. Bastys, I. Pastoriza-Santos, B. Rodriguez-Gonzalez, R. Vaisnoras, L.M. Liz-Marzan, Formation of silver nanoprisms with surface plasmons at communication wavelengths, Adv. Funct. Mater. 16 (2006) 766–773.
[48] S.Q. Song, B. Cheng, N.S. Wu, A.Y. Meng, S.W. Cao, J.G. Yu, Structure effect of graphene on the photocatalytic performance of plasmonic Ag/Ag_2CO_3-rGO for photocatalytic elimination of pollutants, Appl. Catal. B 181 (2016) 71–78.
[49] N. Bao, X. Miao, X. Hu, Q. Zhang, X. Jie, X. Zheng, Novel synthesis of plasmonic Ag/AgCl@TiO_2 continues fibers with enhanced broadband photocatalytic performance, Catalysts 7 (2017) 117.
[50] P. Wang, B.B. Huang, X.Y. Qin, X.Y. Zhang, Y. Dai, J.Y. Wei, M.H. Whangbo, Ag@AgCl. A highly efficient and stable photocatalyst active under visible light, Angew. Chem. Int. Ed. 47 (2008) 7931–7933.
[51] M. Mousavi, A. Habibi-Yangjeh, Ternary g-C_3N_4/Fe_3O_4/Ag_3VO_4 nanocomposites: novel magnetically separable visible-light-driven photocatalysts for efficiently degradation of dye pollutants, Mater. Chem. Phys. 163 (2015) 421–430.
[52] A. Habibi-Yangjeh, A. Akhundi, Novel ternary g-C_3N_4/Fe_3O_4/Ag_2CrO_4 nanocomposites: magnetically separable and visible-light-driven photocatalysts for degradation of water pollutants, J. Mol. Catal. A-Chem. 415 (2016) 122–130.
[53] A. Akhundi, A. Habibi-Yangjeh, Codeposition of AgI and Ag_2CrO_4 on g-C_3N_4/Fe_3O_4 nanocomposite: novel magnetically separable visible-light-driven photocatalysts with enhanced activity, Adv. Powder Technol. 27 (2016) 2496–2506.
[54] H. Choi, S.J. Ko, Y. Choi, P. Joo, T. Kim, B.R. Lee, J.W. Jung, H.J. Choi, M. Cha, J.R. Jeong, I.W. Hwang, M.H. Song, B.S. Kim, J.Y. Kim, Versatile surface plasmon resonance of carbon-dot-supported silver nanoparticles in polymer optoelectronic devices, Nat. Photonics 7 (2013) 732–738.
[55] Y.J. Cui, Z.X. Ding, P. Liu, M. Antonietti, X.Z. Fu, X.C. Wang, Metal-free activation of H_2O_2 by g-C3N4 under visible light irradiation for the degradation of organic pollutants, Phys. Chem. Chem. Phys. 14 (2012) 1455–1462.
[56] L.M. Yang, L.E. Yu, M.B. Ray, Photocatalytic oxidation of paracetamol: dominant reactants, intermediates, and reaction mechanisms, Environ. Sci. Technol. 43 (2009) 460–465.